

Investigation of mixing for Ejected Material in Supernova Remnant Cas A

Yasuhide Matsuo¹, Masa-aki Hashimoto¹, Akira Dohi¹ and Kenzo Arai²

¹Department of Physics, Kyushu University, Fukuoka, Japan

²Department of Physics, Kumamoto University, Kumamoto, Japan

Abstract

Recent observations of Cas A suggest that the element distributions for silicon (Si) and iron (Fe) are very peculiar: Fe locates in front of Si. We investigate the formation of the remnant of Cas A and hydrodynamical calculations are performed from the beginning of explosion to the present stage. It is found that the Rayleigh-Taylor instability is developed from the boundary between hydrogen and helium layers. The instability between Si and Fe layers is not grown enough to induce the observed matter mixing if only the mass loss is included during the red super giant stage.

Keywords: Circumstellar evolution, stellar evolution, supernova, abundances, hydrodynamics

Introduction

The young supernova remnant in our Galaxy, Cassiopeia A (Cas A), is the brightest radio source so far [1]. On the other hand, it has been observed in possible bands of the spectrum: radio [2], infrared [3], visible [4] and X-ray [5]. The yields of hydrodynamical simulations are compared in detail with the observed properties. Therefore, Cas A becomes one of the main targets for numerical studies of supernova and progenitor. The central object has been identified to be a neutron star; Ref. [6] has analyzed the X-ray spectra of Cas A, and gives the effective temperature ($T_{\text{eff}} = 1.61_{-0.05}^{+0.14} \times 10^6$ K) and possible regions occupied by mass and radius relations. Since Cas A is the isolated remnant, uncertainty of mass and radius relation could be large. The lowest mass obtained by χ^2 fitting is about $1.5M_{\odot}$. However, the progenitor of the object is not identified; from the observations of the remnant, the progenitor is at least considered to be a massive star. As a result, the mechanism to produce enough energy to explode the progenitor star is not known well and the structure of the compact object is also controversial [7]. Furthermore, Ref. [8] reported the observation of T_{eff} for Cas A in recent 10 years, where the rapid decrease in T_{eff} during the years shows that the transition to nucleon superfluidity occurs.

The observations of X-ray from Cas A indicate that the progenitor exploded in A.D. 1681 ± 19 [9]. The distance to Cas A is determined to be $3.4_{-0.1}^{+0.3}$ kpc [10] and its size is 2 – 3 pc. Although the type of the supernova for Cas A was inferred to be Ib/c [11], it has been finally identified to be type IIb from the observation of light echo [12], which indicates the explosion of a helium star. The estimated mass of the progenitor star is in the range of 15 – 25 M_{\odot} for the main sequence era [13, 14]. The ejecta includes radioactive nuclei ^{44}Ti and ^{56}Ni whose masses have been obtained [15, 16, 17, 18]. From the studies of supernova 1987A, it is considered that the production process of the abundances can be understood well as far as the spherical explosion is concerned [19]. On the contrary, non-spherical explosion should result in for all supernovae, which is concluded by multi-dimensional numerical simulations [20].

The observations indicate peculiar regions where Fe distributes outside the Si-rich layer [21]. Recent observations of the 3D structure of Cas A [18, 22, 23] also show the same kind of distributions. Since this observational evidence cannot be explained in terms of a spherical explosion model, some kinds of mixing should occur in large scale. Here, we infer the mechanism of the mixing processes: the Rayleigh-Taylor instabilities inside the star [24], interactions between supernova shock and circumstellar medium [25], and the non-spherical explosion such as jets and/or standing accretion shock instability [20, 26]. In particular, we notice the fact that the Rayleigh-Taylor instability develops for an interface between two fluids of different densities, which occurs when the lighter fluid presses the heavier one [27, 28, 29]. This situation is expected to be realized inside a progenitor star. However, since a detailed calculation from an early stage of a progenitor to the explosion does not exist due to numerical difficulty of simulations, some calculations having a model of circumstellar gas, progenitor, and explosion should be desirable.

In the present paper, we investigate whether mixing occurs between Si- and Fe-layers due to the Rayleigh-Taylor instability during supernova explosion, where we adopt a presupernova model and construct circumstellar matter ejected from a progenitor. Two dimensional hydrodynamical simulations are performed from the onset of the explosion to the present remnant phase of Cas A by extending the technical method used for the mixing in supernova 1987A [24, 30].

1 Basic Equations

Let D/Dt be the Lagrange differentiation ($D/Dt = \partial/\partial t + v \cdot \nabla$), which varies along the fluid particle with the velocity v . The non-relativistic equations of fluid dynamics relevant for the simulations are as follows [31]

$$\frac{D\rho}{Dt} = -\rho \nabla \cdot v, \quad (1)$$

$$\rho \frac{Dv}{Dt} = -\nabla P - \rho \nabla \left(\Phi - \frac{GM_{\text{pt}}}{r} \right), \quad (2)$$

$$\rho \frac{D}{Dt} \left(\frac{e}{\rho} \right) = -P \nabla \cdot v, \quad (3)$$

where ρ , P , e and v are the density, pressure, internal energy density, velocity of fluid, G is the gravitational constant and M_{pt} is the mass of the point source at the center. Self gravitational potential Φ is obtained from solving the following Poisson equation

$$\nabla^2 \Phi = 4\pi G \rho. \quad (4)$$

We define the radius R_{ph} of the photosphere to be

$$\int_{R_{\text{ph}}}^{\infty} \rho(r) \kappa_{\text{es}} dr = \frac{2}{3},$$

where κ_{es} is the opacity due to the electron scattering: $\kappa_{\text{es}} = 0.20(1 + X) \text{ cm}^2 \text{ g}^{-1}$ with the hydrogen mass fraction X .

The above set of equations (1)–(4) are closed with an equation of state included. Inside the photosphere, $r \leq R_{\text{ph}}$, we take a mixture of radiation and gases composed of electrons and ions:

$$\begin{aligned} P &= P_{\text{rad}} + P_{\text{gas}}, \\ e &= 3P_{\text{rad}} + \frac{3}{2}P_{\text{gas}}, \end{aligned}$$

with

$$\begin{aligned} P_{\text{rad}} &= \frac{1}{3}aT^4, \\ P_{\text{gas}} &= \frac{R}{\mu}\rho T, \end{aligned}$$

where T is the temperature, a is the radiation constant, R is the gas constant and μ is the mean molecular weight.

Since outside R_{ph} radiation becomes free, we set

$$\begin{aligned} P &= P_{\text{gas}}, \\ e &= \frac{3}{2}P_{\text{gas}}. \end{aligned}$$

Supernova explosions make the high temperature region, where explosive nucleosynthesis occurs significantly. For a high temperature region above 5×10^9 K, all materials are in nuclear statistical equilibrium. When $T \leq 5 \times 10^9$ K, nuclear reactions build up elements toward Fe-group nuclei. Therefore, we take into account 14 species of nuclei: p , ^4He , ^{12}C , ^{16}O , ^{20}Ne , ^{24}Mg , ^{28}Si , ^{32}S , ^{36}Ar , ^{40}Ca , ^{44}Ti , ^{48}Cr , ^{52}Fe and ^{56}Ni . The abundance flow (advection) can be followed by solving (1) for individual elements k with the mass fraction X_k , where $X_k = \rho_k/\rho$.

Once ρ and T are determined by solving hydrodynamic equations (1)–(4), the nuclear reaction rates are evaluated and abundance changes can be calculated. Consequently, the generated nuclear energies are added to the internal energy. In the numerical calculations, we utilize the Zeus-2D code [32] from the onset of the explosion to the present era.

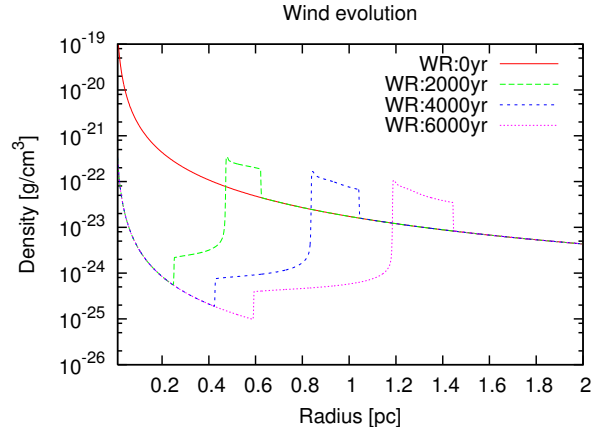


Figure 1: Evolution of WR wind and RSG wind. Wind shells are formed at the boundary between the two winds.

2 Initial Models

2.1 Construction of the Circumstellar Matter

It is observed that a progenitor of Cas A had lost most hydrogen-rich envelope before the explosion [12]. We may infer that the progenitor was a Wolf-Rayet (WR) star: the progenitor experiences three stellar evolutionary stages from main sequence (MS) via redsuper giant (RSG) finally to WR.

According to the calculation of stellar evolution [25], the RSG stage continues over 0.6 Myr with a typical wind velocity 10 km s^{-1} . The boundary between the MS and RSG winds locates at about 6 pc, which is compared to the forward shock front of 2.5 pc [33]. Therefore, we neglect the effects of the MS wind on the evolution of stellar wind.

If we assume the RSG wind is spherical and steady [34], then the density in the wind is written from (1) as

$$\rho(r) = \frac{\dot{M}_{\text{RSG}}}{4\pi r^2 v_{\text{RSG}}}, \quad (5)$$

where \dot{M}_{RSG} is the mass loss rate and v_{RSG} is the velocity of the RSG wind. From the stellar evolution calculations [35], we adopt $\dot{M}_{\text{RSG}} = 1.54 \times 10^{-5} M_{\odot} \text{yr}^{-1}$, $v_{\text{RSG}} = 4.7 \text{ km s}^{-1}$ and $T_{\text{RSG}} = 10^3 \text{ K}$. Under the above condition of the RSG wind, the WR winds are advected [36] with $\dot{M}_{\text{WR}} = 9.6 \times 10^{-6} M_{\odot} \text{yr}^{-1}$, $v_{\text{WR}} = 1.7 \times 10^3 \text{ km s}^{-1}$ and $T_{\text{WR}} = 10^4 \text{ K}$.

We calculate the spherical stellar wind from 0.01 to 2 pc with the 2000 equally stretched meshes. The evolution of the winds is shown in Fig. 1. Since the WR wind becomes three orders in magnitude faster than the RSG wind, the WR wind pushes the back of the RSG wind. Consequently, high density shells (WR+RSG shells) are formed around the boundary between the two winds.

It has been reported that the duration t_{WR} of the WR stage could be less than about 3500 yr [37]. Taking into account the uncertainty in t_{WR} , we consider two cases for the duration $t_{\text{WR}} = 0$ (RSG only) and 2000 yr.

Table 1: Models associated to stellar winds. t_{WR} is the duration of the WR stage, E_{in} is the input energy of explosion, R_{fs} and R_{rs} are the locations of the forward and reverse shocks, respectively

Models	WR0E2	WR0E3	WR0E4	WR2E2	WR2E3	WR2E4
$t_{\text{WR}} (10^3 \text{ yr})$	0	0	0	2	2	2
$E_{\text{in}} (10^{51} \text{ erg})$	2	3	4	2	3	4
$R_{\text{fs}} (\text{pc})$	1.8	2.1	2.5	1.9	2.3	2.6
$R_{\text{rs}} (\text{pc})$	1.3	1.6	1.7	1.0	1.2	1.3

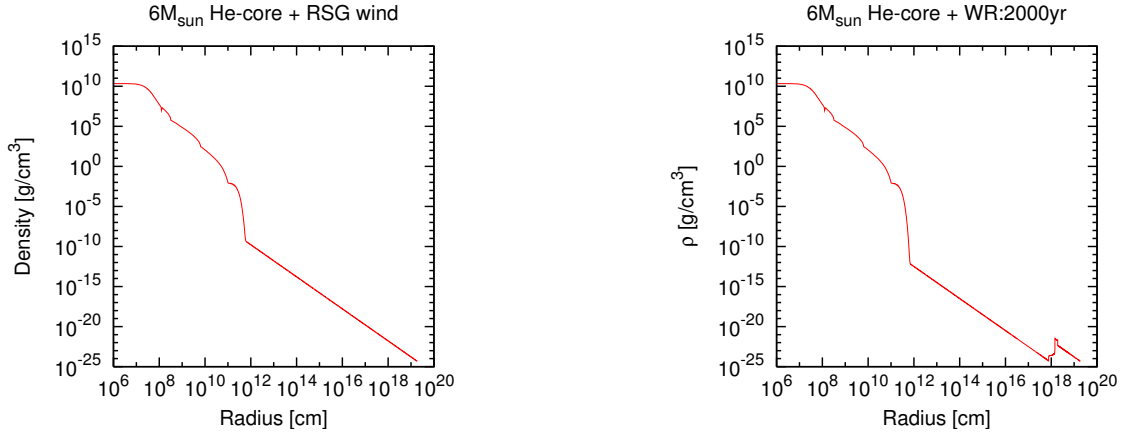


Figure 2: Density distribution of the initial models for $t_{\text{WR}} = 0$ (left panel) and 2000 yr (right panel). The original presupernova core of $6M_{\odot}$ lies inside 10^{11} cm. The knob around 10^{18} cm in the right panel is ascribed to the WR+RSG shell.

2.2 Observational Constraints Due to One Dimensional Simulations

We adopt the presupernova model of a He-core of $6M_{\odot}$ [19] which corresponds to MS of around $20 M_{\odot}$. This model is consistent with the evaluation of the progenitor of Cas A [13, 14]. Our initial models are constructed by connecting this presupernova model with the WR and RSG winds described in the last subsection. Figure 2 shows the density distribution of the initial models. The left panel indicates the case $t_{\text{WR}} = 0$ and the right one is the case $t_{\text{WR}} = 2000$ yr. Note that there appears a knob around 10^{18} cm, which is ascribed to the WR + RSG shell.

Table 1 gives the positions R_{fs} of the forward shock and R_{rs} of the reverse shock for models with the input energy of explosion $E_{\text{in}} = 2 - 4 \times 10^{51}$ erg in two cases. The observed locations are $R_{\text{fs}} = 2.5 \pm 0.2$ pc and $R_{\text{rs}} = 1.6 \pm 0.2$ pc in Cas A [33]. Therefore, only a model WR0E4 is fitted to the observations of both R_{fs} and R_{rs} , which is consistent with the previous study [38]. As a consequence, we examine matter mixing due to the Rayleigh-Taylor instabilities for this model.

3 Rayleigh-Taylor Instabilities

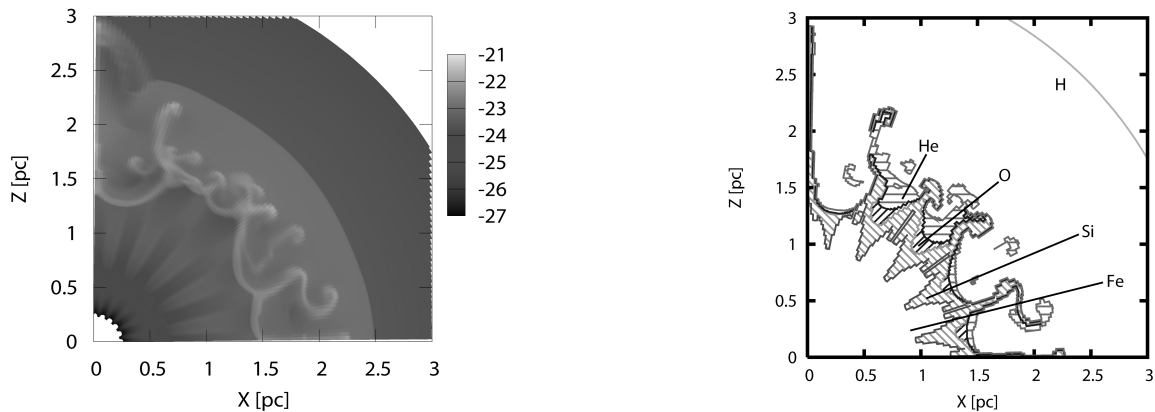


Figure 3: Contours of the logarithm of density in units of g cm^{-3} (left panel) and the distribution of major elements (right panel) at $t = 330$ yr after the explosion. The dashed region of Si includes O, where the mass fraction of Si is larger than 5 % of that of O. The regions of He and O are occupied by almost these elements.

We perform two dimensional simulations of supernova explosion for the initial model WR0E4. Our region of

calculation is divided into 1000×100 meshes in the $r\theta$ plane. When the shock wave passes the boundary between C+O and He-rich layers at $t = 3.9$ s after the explosion, we specify perturbations in the r -component of velocities as

$$\delta v_r = \epsilon v_r \cos(20\theta), \quad (6)$$

where we set $\epsilon = 0.1$. The Rayleigh-Taylor instability is judged from the criterion [39]

$$\nabla\rho \cdot \nabla P < 0. \quad (7)$$

This condition is satisfied in most regions of the boundary layers after the shock passes through.

During the propagation of the shock wave, we follow the abundance change using an α network code [40] which contains 13 nuclei from ${}^4\text{He}$ to ${}^{56}\text{Ni}$. Furthermore to evaluate the amount of radio actives, nucleosynthesis is calculated in detail for tracer particles using the post process method with a large network code [31] of 464 nuclei. The produced amounts are found to be ${}^{44}\text{Ti}$ of $1.3 \times 10^{-4} M_\odot$ and ${}^{56}\text{Ni}$ of $0.123 M_\odot$, whose values are consistent with the observed abundances [15, 17, 18].

Figure 3 shows our results of simulations at $t = 330$ yr after the explosion. The left panel indicates the density contours, where the instability develops at $r \simeq 0.4$ and 1.6 pc. The former region is attributed to the boundary between original O- and Si-rich layers. The latter corresponds to the boundary between H- and He-rich layers. We note that in the deep O-rich layer, both Si and Fe are produced through the explosive O-burning. Most Fe are daughters of radioactive nuclei ${}^{56}\text{Ni}$. As seen from the right panel, no mixing occurs between Si and Fe in the present simulations.

4 Discussion

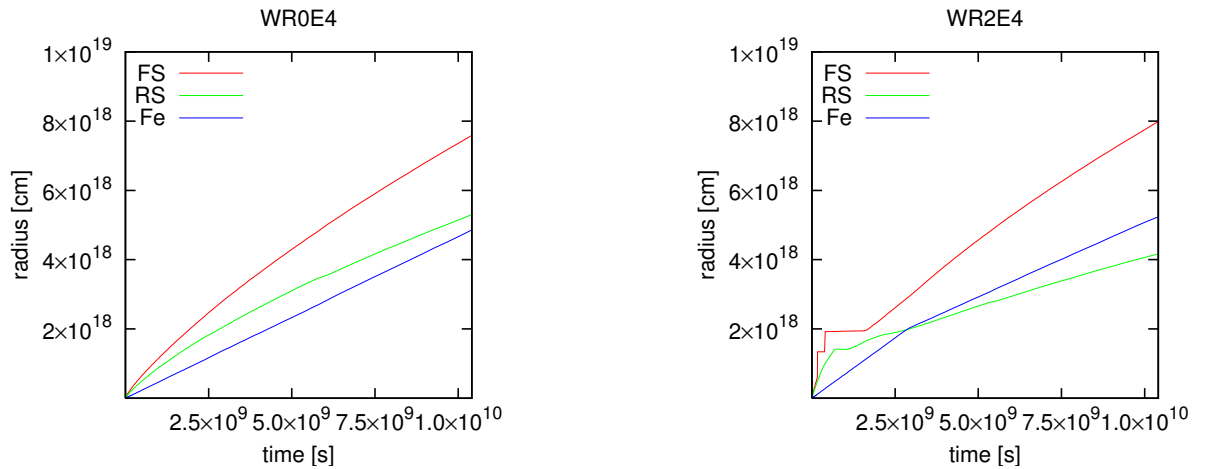


Figure 4: Development of the forward shock (FS), the reverse shock (RS) and the surface of the Fe layer (Fe) for models of WR0E4 (left panel) and WR2E4 (right panel). The Fe-surface overtakes RS at $t \simeq 2.5 \times 10^9$ s in WR2E4, where jumps near the location of FS appear during $(0.16 - 1.6) \times 10^9$ yr. Since FS collides with the WR+RSG shell, it is difficult to determine the position of FS. After 1.6×10^9 yr, we can exactly calculate that of FS because it completely passes through the WR+RSG shell.

We have performed two dimensional simulations of supernova explosion and followed the abundance change during the propagation of the shock wave. Adopting a specific circumstellar model, we cannot find mixing between Si and Fe-layers due to the Rayleigh-Taylor instability. However, after the shock passage, instability criterion (7) always holds in a region of abundant Si and Fe. We would suggest possible issues for the mixing to occur.

Different initial models are worthwhile studying. As seen from Fig. 3, the Si layer extends only to about 2 pc, which is inconsistent with the observations. This is ascribed to the distribution of the circumstellar matter. Figure 4 shows development of the forward shock, the reverse shock and the surface of Fe layer for models of WR0E4 (left panel) and WR2E4 (right panel). It is clear that there appears the difference in the way of shock propagation. In particular, the Fe layer catches up with the reverse shock at $t \simeq 2.5 \times 10^9$ s due to the collision of shocks and WR+RSG shell. Much

larger scale mixing would be expected because the Rayleigh-Taylor instability is developed at the front of the reverse shock [41]. Our model WR0E4 could be inappropriate to induce the hydrodynamical instabilities in circumstellar medium. Therefore, shock propagation should be examined for different distributions of circumstellar medium.

The resolution of calculations should be refined. We have divided the region into 1000×100 domains. It is difficult to follow both the shock wave outside the star and the Fe layers confined deep inside the star. Simulations of a core collapse supernova with higher resolution by using adaptive mesh refinement [41] may imply that our calculation is not enough to resolve the instabilities for matter mixing. Large scale mixing could be realized through the three dimensional calculations as suggested by the observations. It is proposed that the Rayleigh-Taylor instability could be more sufficiently developed in three dimensional calculations than two dimensional ones [42]. Matter mixing could be originated from the mechanism of core collapse supernova. For example, standing accretion shock instability may induce the significant mixing between Si and Fe layers [20].

Acknowledgments

This work was supported by JSPS KAKENHI Grant Numbers 24540278 and 15K05083.

References

- [1] Ryle, M.; Smith, F. G. **1948**, *162*, 462–463.
- [2] Anderson, M.; Rudnick, L.; Leppik, P.; Perley, R.; Braun, R. **1991**, *373*, 146–157.
- [3] Krause, O.; Rieke, G. H.; Birkmann, S. M.; Le Floch, E.; Gordon, K. D.; Egami, E.; Biegging, J.; Hughes, J. P.; Young, E. T.; Hinz, J. L.; Quanz, S. P.; Hines, D. C. *Science* **2005**, *308*, 1604–1606.
- [4] Fesen, R. A.; Gundersen, K. S. **1996**, *470*, 967–980.
- [5] Willingale, R.; Bleeker, J. A. M.; van der Heyden, K. J.; Kaastra, J. S. **2003**, *398*, 1021–1028.
- [6] W. C. G. Ho & C. O. Heinke, 2009, *Nature*, *462*, 71–73.
- [7] Pérez-Rendón, B.; García-Segura, G.; Langer, N. **2009**, *506*, 1249–1259.
- [8] Heinke, C. O. & Ho, W. C. G. 2010, , *L719*, 167–171.
- [9] Fesen, R. A.; Hammell, M. C.; Morse, J.; Chevalier, R. A.; Borkowski, K. J.; Dopita, M. A.; Gerardy, C. L.; Lawrence, S. S.; Raymond, J. C.; van den Bergh, S. **2006**, *645*, 283–292.
- [10] Reed, J. E.; Hester, J. J.; Fabian, A. C.; Winkler, P. F. **1995**, *440*, 706–721.
- [11] Fesen, R. A.; Becker, R. H.; Blair, W. P. **1987**, *313*, 378–388.
- [12] Krause, O.; Birkmann, S. M.; Usuda, T.; Hattori, T.; Goto, M.; Rieke, G. H.; Misselt, K. A. *Science* **2008**, *320*, 1195–1197.
- [13] Young, P. A.; Fryer, C. L.; Hungerford, A.; Arnett, D.; Rockefeller, G.; Timmes, F. X.; Voit, B.; Meakin, C.; Eriksen, K. A. **2006**, *640*, 891–900.
- [14] Lee, J.-J.; Park, S.; Hughes, J. P.; Slane, P. O. **2014**, *789*, 7 (11pp.).
- [15] Vink, J.; Laming, J. M.; Kaastra, J. S.; Bleeker, J. A. M.; Bloemen, H.; Oberlack, U. **2001**, *560*, L79–L82.
- [16] Willingale, R.; Bleeker, J. A. M.; van der Heyden, K. J.; Kaastra, J. S.; Vink, J. **2002**, *381*, 1039–1048.
- [17] Eriksen, K. A.; Arnett, D.; McCarthy, D. W.; Young, P. **2009**, *697*, 29–36.
- [18] Milisavljevic, D.; Fesen, R. A. *Science* **2015**, *347*, 526–530.
- [19] Hashimoto, M. *Prog. Theor. Physics* **1995**, *94*, 663–736.
- [20] Orlando, S.; Miceli, M.; Pumo, M. L.; Bocchino, F. **2016**, *822*, 22 (18pp.).
- [21] Vink, J. **2004**, *48*, 61–67.
- [22] DeLaney, T.; Rudnick, L.; Stage, M. D.; Smith, J. D.; Isensee, K.; Rho, J.; Allen, G. E.; Gomez, H.; Kozasa, T.; Reach, W. T.; Davis, J. E.; Houck, J. C. **2010**, *725*, 2038–2058.
- [23] Grefenstette, Brian W, et al. **2017**, *834*, id.19, 13pp.
- [24] Hachisu, I.; Matsuda, T.; Nomoto, K.; Shigeyama, T. **1990**, *358*, L57–L61.
- [25] Pérez-Rendón, B.; García-Segura, G.; Langer, N. **2009**, *506*, 1249–1259.
- [26] Blondin, J. M.; Mezzacappa, A.; DeMarino, C. **2003**, *584*, 971–980.
- [27] Rayleigh, Lord (John William Strutt) (1883). *Proceedings of the London Mathematical Society*. 14: 170–177.

- [28] Taylor, Sir Geoffrey Ingram (1950). Proceedings of the Royal Society of London. Series A, Mathematical and Physical Sciences. 201 (1065): 192–196.
- [29] Chandrasekhar, Subrahmanyan (1981). Hydrodynamic and Hydromagnetic Stability. Dover Publications. ISBN 978-0-486-64071-6.
- [30] Nagataki, S.; Shimizu, T. M.; Sato, K. **1998**, *495*, 413–423.
- [31] Ono, M.; Hashimoto, M.; Fujimoto, S.; Kotake, K.; Yamada, S. **2009**, *122*, 755–777.
- [32] Stone, J. M.; Norman, M. L. **1992**, *80*, 753–790.
- [33] Gotthelf, E. V.; Koralesky, B.; Rudnick, L.; Jones, T. W.; Hwang, U.; Petre, R. **2001**, *552*, L39–L43.
- [34] Nozawa, T.; Kozasa, T.; Tominaga, N.; Maeda, K.; Umeda, H.; Nomoto, K.; Krause, O. **2010**, *713*, 356–373.
- [35] Hirschi, R.; Meynet, G.; Maeder, A. **2004**, *425*, 649–670.
- [36] Nugis, T.; Lamers, H. J. G. L. M. **2000**, *360*, 227–244.
- [37] Schure, K. M.; Vink, J.; García-Segura, G.; Achterberg, A. **2008**, *686*, 399–407.
- [38] van Veelen, B.; Langer, N.; Vink, J.; García-Segura, G.; van Marle, A. J. **2009**, *503*, 495–503.
- [39] Takabe, H. **1993**, *69*, 1285–1300.
- [40] Mueller, E. **1986**, *162*, 103–108.
- [41] Kifonidis, K.; Plewa, T.; Scheck, L.; Janka, H.-T.; Müller, E. **2006**, *453*, 661–678.
- [42] Noro, A.; Ohta, T.; Yamashita, K.; Miyaji, S. **2002**, *2327*, 207–218.